Journal of Medicinal Chemistry

Article

G-Protein-Coupled Receptor Affinity Prediction Based on the Use of a Profiling Dataset: QSAR Design, Synthesis, and Experimental Validation

Catherine Rolland, Rafael Gozalbes, Eric Nicola, Marie-France Paugam, Laurent Coussy, Frdrique Barbosa, Dragos Horvath, and Frdric Revah

J. Med. Chem., **2005**, 48 (21), 6563-6574• DOI: 10.1021/jm0500673 • Publication Date (Web): 22 September 2005

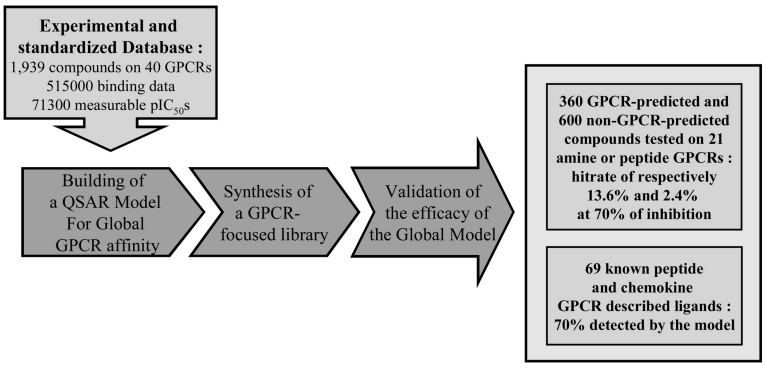

More About This Article

Additional resources and features associated with this article are available within the HTML version:

- Supporting Information
- Links to the 5 articles that cite this article, as of the time of this article download
- Access to high resolution figures
- Links to articles and content related to this article
- Copyright permission to reproduce figures and/or text from this article

View the Full Text HTML

Journal of Medicinal Chemistry is published by the American Chemical Society. 1155 Sixteenth Street N.W., Washington, DC 20036

G-Protein-Coupled Receptor Affinity Prediction Based on the Use of a Profiling Dataset: QSAR Design, Synthesis, and Experimental Validation

Catherine Rolland,*,† Rafael Gozalbes,† Eric Nicolaï,† Marie-France Paugam,† Laurent Coussy,‡ Frédérique Barbosa,† Dragos Horvath,†,§ and Frédéric Revah†

Cerep, 128 rue Danton, 92500 Rueil-Malmaison, France, and Cerep, Le Bois l'Evêque, 86600 Celle l'Evescault, France

Received January 24, 2005

A QSAR model accounting for "average" G-protein-coupled receptor (GPCR) binding was built from a large set of experimental standardized binding data (1939 compounds systematically tested over 40 different GPCRs) and applied to the design of a library of "GPCR-predicted" compounds. Three hundred and sixty of these compounds were randomly selected and tested in 21 GPCR binding assays. Positives were defined by their ability to inhibit by more than 70% the binding of reference compounds at 10 μM. A 5.5-fold enrichment in positives was observed when comparing the "GPCR-predicted" compounds with 600 randomly selected compounds predicted as "non-GPCR" from a general collection. The model was efficient in predicting strongest binders, since enrichment was greater for higher cutoffs. Significant enrichment was also observed for peptidic GPCRs and receptors not included to develop the QSAR model, suggesting the usefulness of the model to design ligands binding with newly identified GPCRs, including orphan ones.

Introduction

G-protein-coupled receptors (GPCRs) are transmembrane proteins that play a critical role in signal transduction. Members of this superfamily respond to stimuli as diverse as neurotransmitters, hormones, and sensory stimuli such as light, odor, and taste, which selectively activate intracellular signaling events through interaction with heterotrimeric G proteins. As GPCRs are initiators of a cascade of cellular responses via diverse extracellular mediators, they can be used to control cell behavior, when targeted by specific drug molecules. It is estimated that about 50% of currently commercialized drugs are active through their interaction with one of a set of about 30 different GPCRs.[1,2] Also, analysis of the human genome has shown the number of potentially relevant GPCRs for drug discovery to be up to 600, among which 160 receptors have no known ligand (orphan receptors). GPCRs have been classified into three major subfamilies on the basis of their relation to rhodopsin (type A), secretin receptor (type B), and metabotropic receptors (type C).[2,3] Subgroups of family A, which is by far the largest, have been recently defined by Joost and Methner[4] for more accurate phylogenetic analyses to predict possible ligands for orphan receptors.

The determination of the 3-D structure of GPCRs by X-ray crystallography or nuclear magnetic resonance has been hampered by their transmembrane nature. Only one GPCR crystallographic structure has been reported until now, that of bovine rhodopsin.[5] Although this available structural template is widely used for the interpretation of experimental data and for the building of molecular models of other receptors of family A, rhodopsin reveals a low sequence similarity to others GPCRs, limiting its relevance in drug design efforts. More generally, while homology modeling of GPCR structures has been a widely used modeling technique,[6,7] several authors have expressed their skepticism concerning the utility of this approach.[7,8]

In the present study, our objective has been to capture characteristic structural features of GPCR ligands. To reach this goal, we have systematically studied the binding of a set of 1939 diverse compounds to a reference panel of 40 different GPCRs. The compounds used correspond to most marketed drugs, compounds having failed in clinical trials, and reference compounds. The data set was produced in-house under standardized operating procedures and lead to the generation of 515 000 experimental measures and 71 300 measurable IC_{50}s (BioPrint, see ref 9).

In a first step, a "global" quantitative structure−activity relationship (QSAR) model was developed by using the average pIC_{50} value for these 40 GPCRs. In a second step, this model was used to design a library of compounds predicted to display GPCR activity (i.e. rich in structural patterns that are commonly recognized by a majority of GPCRs). Finally, the predicted compounds were synthesized and tested over a set of 21 GPCRs, some belonging to the initial training set, others not belonging to it. These results were compared to that obtained when testing compounds predicted as non-GPCR by the model. We also analyzed the capacity of our model to recognize selective GPCR ligands in contrast to molecules binding to multiple receptors. This study allows us to assess the relevance and limitations of such a global QSAR approach for the design of GPCR-focused libraries.

* To whom correspondence should be addressed. Phone: +33 (0)1 55 94 84 55. Fax: +33 (0)1 55 94 84 10. E-mail: C.Rolland@cerep.fr.
† Cerep, Rueil-Malmaison.
‡ Cerep, Celle l'Evescault.
§ Current address: Institut de Biologie de Lille, CNRS-UMR 8525, 59800 Lille, France.

10.1021/jm0500673 CCC: $30.25
Published on Web 09/22/2005

Table 1. List of 40 GPCR Receptors Included in BioPrint and Used for the Development of the "Global GPCR" QSAR Model

GPCRs	type	family	no. of compds tested	no. of compds with inhibn > 70%	higher pIC_{50} values
5-HT_{1A}	biogenic amine	A19	1813	266	9.3
5-HT_{1B}	biogenic amine	A19	1795	124	9.4
5-HT_{1D}	biogenic amine	A19	1832	58	7.9
5-HT_{2A}	biogenic amine	A17	1776	249	8.5
5-HT_{2B}	biogenic amine	A17	1628	323	8.7
5-HT_{2C}	biogenic amine	A17	1622	207	8.4
5-HT_{4e}	biogenic amine	–	1717	102	8.4
5-HT_6	biogenic amine	A17	1788	155	9.2
5-HT_7	biogenic amine	A19	1797	235	8.7
A_1	biogenic amine	A18	1814	41	8.3
A_{2A}	biogenic amine	A18	1620	49	8.2
α_{1A}	biogenic amine	A17	1850	227	9.2
α_2	biogenic amine	A17	1803	202	8.5
AT_1	peptide	A3	1870	11	8.6
B_2	peptide	A3	1874	2	5.3
β_1	biogenic amine	A17	1867	64	8.6
β_2	biogenic amine	A17	1698	102	9.0
CB_1	cannabinoid	A13	1662	6	6.7
CCK_A	peptide	A6	1872	1	5.2
CCR1	chemokine	A1	1861	2	4.5
CGRP	peptide	B	1728	0	5.3
D_1	biogenic amine	A17	1828	189	9.1
D_2	biogenic amine	A17	1825	166	8.9
D_3	biogenic amine	A17	1612	229	8.6
$D_{4.4}$	biogenic amine	A17	1683	168	8.9
δ	opioide	A4	1837	77	8.3
ET_B	peptide	A7	1860	1	5.3
$GABA_B$	aminobutyric acid	C	1749	10	6.6
H_1	biogenic amine	A18	1778	215	8.7
H_2	biogenic amine	A17	1780	217	7.3
κ	opioid	A4	1751	198	9.7
M_1	biogenic amine	A18	1778	246	9.3
M_2	biogenic amine	A18	1812	217	9.0
M_3	biogenic amine	A18	1850	155	8.7
MC_4	peptide	A13	1841	27	6.7
μ	opioid	A4	1796	166	9.1
NK_1	peptide	A9	1682	25	6.3
V_{1a}	peptide	A6	1857	3	6.9
VIP	peptide	B	1844	5	5.1
Y_1	peptide	A9	1850	8	6.3

Dataset and Activity Variable Used To Develop the QSAR Model. Compounds from the BioPrint collection were tested over the entire panel of GPCR targets described in Table 1, and pIC_{50} values were systematically measured whenever the primary percentage of inhibition value exceeded 30% at 10 μM. Otherwise, compounds were considered as "inactive", and their pIC_{50} value was set by default to 3.5. The activity variable monitored in this study, further on termed as the "global GPCR" or "GPCR" affinity, has been defined as the plain average of the pIC_{50} values of each compound over the entire panel of GPCR targets included in BioPrint [$pIC_{50} = -\log IC_{50}$ (M)]. As it is unlikely to find a compound acting as a potent nanomolar binder on every GPCR target in the panel, the global GPCR affinity is expected to adopt values from 3.5 (inactivity vs all of the GPCRs) to an upper limit below 9. In practice, this GPCR upper value was found to be 5.8 for the compound collection tested. The distribution of global GPCR affinity values was found to be lower than 4.0 for 1541 compounds and equal to or higher than 4.0 for 398 compounds.

For QSAR model-building purposes, the BioPrint compound set was split into a learning set (LS, 1551 compounds representing 80% of the total database) and a validation set (VS, 388 compounds, representing the remaining 20% of the database). Splitting was done such as to ensure an equivalent relative distribution of actives and inactives throughout both sets (around a 20% of compounds had pIC_{50} values ≥ 4.0 for both LS and VS).

QSAR Methodology. A detailed discussion of the technical aspects of this methodology is beyond the purpose of this publication and has been published elsewhere.[10−13]

Descriptors. The elaboration of a QSAR model requires the previous encoding of compound structures as molecular descriptors, which capture information regarding the structural features responsible for the activity under a numerical form. The Cerep proprietary descriptors consist of various 3-D terms of "pharmacophoric" nature, carrying information about the nature and spatial distribution of the various pharmacophore features in a molecule.

(a) Fuzzy Bipolar Pharmacophore Autocorrelograms (FBPA). In order to generate the FBPA of a compound, its atoms are first classified according to their pharmacophoric features (hydrophobicity, aromaticity, hydrogen-bond donor or -acceptor propensity, positive or negative charge). Any atom may possess one or more such features, detected by a feature assignment routine, according to empirical rules. The 21 pairs of these six features are defined (hydrophobic−hydrophobic, hydrophobic−aromatic, etc.). All the atom pairs occurring in a molecule are first assigned to one of these 21 pharmacophore pair categories and furthermore broken down into 12 interatomic-distance-related bins of 1 Å width, going from 3 to 15 Å. This defines a total of 252 classes to which an atom pair may belong, and the fingerprint is thus a 252-dimensional vector in which every component represents the number of atom pairs associated to the given category, averaged over a diverse sample of conformers.[11]

(b) Pharmacophore Type Areas (PTA) report the molecular areas corresponding to each type of pharmacophoric feature (aliphatic, aromatic, hydrogen-bond acceptor and donor, cationic and anionic areas).[10]

(c) Extended Field Overlap (EFO) terms offer a synthetic characterization of the spatial distribution of pharmacophoric features in the molecule: these terms are volume integrals of the pairwise products of local field intensities associated with each of the possible combinations of the pharmacophore types. For these descriptors, a more detailed ("extended") definition of the pharmacophore types is used, featuring 10 rather than six explicit pharmacophore types. For example, the hydrogen bond donor class is further split into "aromatic hydrogen-bond donors" (e.g., indole -NH-), "donors and acceptors" (e.g., alcohol −OH), and "donors only" (e.g., amide −NH).

QSAR Model Building. After the filtering out of constant or strongly intercorrelated ($R^2 > 0.8$) descriptor columns, the final activity-descriptor matrix, aligning each experimental activity against the associated candidate molecular descriptors, is built and fed into the various descriptor selection algorithms in order to find the optimal structure−activity relationships. Synergy models based on two different approaches, linear re-

gression on one hand, and predictive neighborhood behavior on the other, are employed.[12,13]

(a) Linear Models. Learning and validation sets were used to train and validate several thousands of statistically valid linear equations, expressing the estimate of the global GPCR affinity value as linear combinations of molecular descriptors selected by a genetic algorithm (GA).[10] The linear models within each pool were subjected to a diversity analysis procedure in order to discard redundant equations based on roughly similar descriptor choices. This procedure assessed whether some of the different descriptors used by different equations were intercorrelated, and therefore interchangeable.[14] The remaining diverse QSAR equations were further classified by "size" (number of descriptors they include) and statistical performance (root mean square error and correlation coefficient). The best equations of each encountered size were kept on hand for final validation of the VS molecules and for further analysis. Five *consensus* models were also generated as weighted averages of the best models found by the GA, where the contribution of each equation to the consensus model decreases with decreasing R^2.

(b) Predictive Neighborhood Behavior Models (PNB). This approach is based on the "neighborhood behavior" principle (similar structures → similar properties),[15,16] and PNB models tend to extrapolate the property of a novel compound as an average of properties of reference molecules that are shown to be structurally similar, according to a well-defined computed similarity score.[12,13] In addition to the calculated property, the model also returns, for each compound, two confidence thresholds controlling the relative trust in the PNB model prediction: a "density criterion" expressing how well the current compound is surrounded by relevant neighbors, as a function of their dissimilarity to the candidate compound, and a "homogeneity criterion" measuring the (weighed) variance of the property within the set of selected neighbors. A low variance means that, as expected on behalf of the similarity principle, the selected neighbors actually have similar properties. Good density and homogeneity scores suggest the prediction for a given compound to be reliable, as this molecule is shown to have many neighbors of roughly identical properties and is therefore likely to display a similar behavior as well.

(c) Synergy Models. The calibration of a synergy model consists of finding, with regard to the confidence indices of the PNB prediction, an optimal balance of weights for the linear vs the PNB prediction, such that the returned "synergy" estimations (weighted averages of the two independent linear and PNB predictions, respectively) are as close as possible to the experimental values.[10]

QSAR Modeling. A computational quantitative structure−activity model was built and validated by tools specifically developed to process the learning and validation sets of the structures and corresponding pharmacological profiles included in the BioPrint database.[9,10] In a first step, the methodology consists of building two sets of "parent" models. The first set of parents consists of *predictive equations*: a series of optimal linear equations, obtained by multilinear regression coupled to a genetic-algorithm-driven descriptor selection process. The second series of parents consists of predictive neighborhood behavior (PNB) models, estimating the properties of a compound as a weighted average of properties of its closest neighbors among reference compounds in structural space, according to a tunable similarity metric. The final models are "synergy" approaches, combining the predictions of two conceptually independent parent approaches, based on an equation and respectively on neighborhood behavior, to return a more accurate prediction as a weighted average of the estimates provided by each parent.[10]

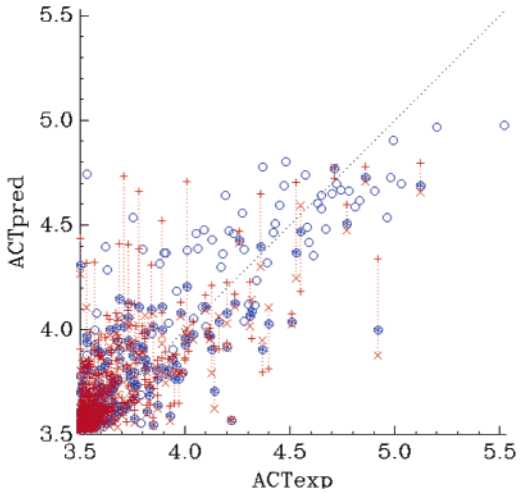

Figure 1. Experimental ("ACTexp") versus predicted values ("ACTpred") for the GPCR average activity of the validation set (VS). Circles mark the position of the synergy model predictions: when both linear and PNB predictions are available, the corresponding marker is spiked. By contrast, hollow blue circles mark the predicted values for the molecules failing to be predicted by the PNB approach (the case when the synergy predictions equal the linear model-based prediction). When both linear and PNB values exist, the dotted red bars span the range between the predicted values of the linear (red plus sign) and PNB models (red x), respectively.

QSAR Model Analysis. The QSAR builder generated several linear models (containing 26−39 descriptors) and PNB models (87−116 descriptors). Synergy models obtained by combination of the best linear and PNB approaches showed, as expected, a better predictive performance than any of their parents taken separately. The best global GPCR synergy model (R^2 = 0.74−0.67 and rms = 0.20−0.24 for the LS and VS, respectively) was further used for this study (the values for the LS and VS of the best linear model were R^2 = 0.71−0.63 and rms = 0.24−0.29 respectively, and R^2 = 0.65−0.61 and rms = 0.22−0.24 for the best PNB model). Figure 1 shows the comparison between predicted and experimental pIC_{50} values for the validation set. Without going into further details, it is worth noting that aromatic−positive charge pairs within different distance bins appear among the key molecular descriptors used in this model, standing for a well-known aromatic−cation pharmacophore pattern that is familiar to GPCR ligands (examples of such pattern are described in the literature for various GPCRs[17−20]). Nevertheless, the model does not restrain the selection of molecules according to such standard criteria, since there were compounds predicted as non-GPCR and experimentally found as inactive on the panel of the 21 GPCRs, despite a structure containing a positive charge

Table 2. Percentages of Learning Set (LS) Molecules and Validation Set (VS) Molecules Classified in Each of the Four Categories [Correctly Predicted Inactives (L^{exp}, L^{pred}), Correctly Predicted Actives (H^{exp}, H^{pred}), Inactives Predicted To Be Active (False Positives) (L^{exp}, H^{pred}), and Actives Predicted To Be Inactive (False Negatives) (H^{exp}, L^{pred})] According to the "Global GPCR" QSAR Model[a]

	L^{expt} (LS/VS)	H^{expt} (LS/VS)	
L^{pred} (LS/VS)	73.4%/71.9%	2.7%/2.6%	NPV = 96.5%/96.5%
H^{pred} (LS/VS)	6.1%/7.5%	17.8%/18.0%	PPV = 74.6%/70.6%
	Sp = 92.4%/90.6%	Sn = 86.8%/87.4%	*A* = 91.2%/89.9%

[a] A confusion matrix summarizing the performance of the "global GPCR" QSAR model is presented. The "L" and "H" refer to the low- and high-affinity classes, with cutoff value of 4.0, and "exp" and "pred" refer to experimental and predicted values. Sn, Sp, PPV, and NPV stand respectively for "sensitivity" (percentage of experimental positives predicted as positives), "specificity" (percentage of correctly predicted as nonbinders), "positive probability value" (probability that a predicted binder will actually a binder), and "negative probability value" (probability that a predicted nonbinder will actually be a nonbinder). The "% efficacy" of a predicted class stands for its contents (%) in compounds of the same experimental class, while "% found" and "sensitivity" represent the percentages of members of a given experimental class that were correctly classified by the prediction. The lower right box shows the accuracy (*A* = overall percentage of correctly predicted compounds).

not far from an aromatic ring. The model also includes, among others, a positive contribution of the total number of aromatic rings in a molecule, and negative contributions from the (square of the) total van der Waals surface areas associated with these same aromatic groups and the presence of aromatic−hydrogen-bond acceptor pairs within a distance between 4 and 5 Å.

A further, more intuitive grasp of the QSAR model quality can be obtained by using a binary classification statistics or confusion matrix in terms of "H(igh)" and "L(ow)" average activity values (Table 2). Compounds with a global GPCR pIC_{50} score below 4.0 were considered as "inactive" (and formally assigned to the L^{exp} class), by contrast to the "actives" that show some significant binding with respect to at least one of the GPCRs, so that their pIC_{50} values exceed 4.0 (H^{exp} class). Similarly, compounds with predicted pIC_{50} higher than 4.0 were therefore considered "predicted active" (of the H^{pred} class), by contrast to the "predicted inactive" ordered into the L^{pred} category. Within the validation set, the activity class predicted by the model matched the experimental activity class of the compound in 89.9% of the cases. Out of the actual "actives" present in the validation set, 87.4% were correctly predicted to be active, whereas 90.6% of the real "inactive" were correctly recognized as such by the model. On the other hand, whenever the model predicted a compound to be active, it turned out to be right in 70.6% of the cases, whereas 96.5% of the predicted inactive turned out to be inactive indeed. In other words, a medicinal chemist screening only the category of N_{act} predicted actives (99 compounds) rather the entire validation set of N_{VS} (388 compounds) would have discovered 87.5% of all the actives that were available, while only 29.3% of the tested molecules would have turned out to be inactive.

Library Design and Synthesis. To assess the usefulness of the global QSAR approach, the model was used to design and synthesize a GPCR-focused library. On one hand, the model was employed to screen for putative GPCR actives (using a criterion of predicted $pIC_{50} \geq 4.0$) within a previously synthesized 16 000-compound diverse library. On the other hand, 50 virtual focused libraries of 200 compounds each were constructed around scaffolds derived from in-house medicinal chemistry know how, and the resulting compounds were then prioritized by the global QSAR model. After analysis of the prediction results for each of the virtual compounds, the chosen compounds were synthesized. These combined approaches yielded a library of 2400 compounds predicted as GPCR-active by the global QSAR model.

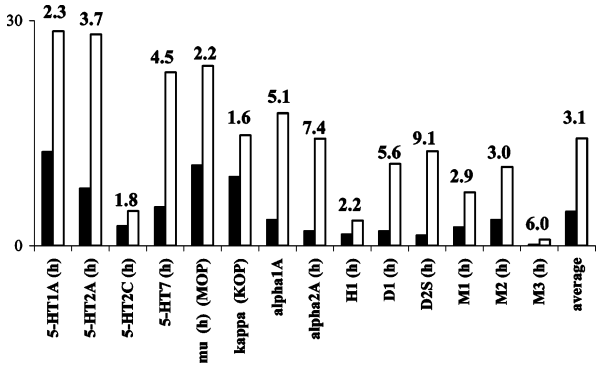

Figure 2. Experimental binding results—at 70% of inhibition at 10 μM—of the 960 compounds (240 compounds from the GPCR-predicted library plus 720 compounds from a general diverse library) on 14 GPCRs. White bars correspond to the hit rates of the GPCR-oriented library and black ones to those of the diversity library. The added values correspond to the hit rate enhancement between these two sets of compounds for each receptor.

Experimental Validation of the Library. To validate the relevance of the methodology, a 10% sample of the proposed GPCR library (240 randomly selected products) was experimentally assayed for binding on a panel of diverse GPCRs and compared to a sample of a general library taken as reference (720 randomly chosen products). We initially profiled these 960 compounds on a set of 14 receptors (5-HT_{1a}, 5-HT_{2a}, 5-HT_{2c}, 5-HT_7, μ, α_{1A}, α_{2A}, κ, M_1, M_2, M_3, D_1, D_2, H_1) (Table 1), chosen among those having the highest hit rates within BioPrint and representing a variety of GPCR subfamilies (A4, A17, A18, A19).[4]

The set of 960 compounds was tested at 10 μM on each receptor. Figure 2 compares the global hit rates with respect to all the targets of the two subsets of molecules, where "hits" are defined as leading to at least 70% inhibition of binding of the reference radioligand when assayed at 10 μM. This stringent threshold allowed us to focus on the most robust hits. The global hit rate of the GPCR library subset reached 14.3%, which represented a 3.1-fold average hit rate enhancement with respect to the 4.6% rate of the general library subset. Receptor-specific hit rate enhancements ranged from 1.6 (in the case of the κ opioid receptor) up to 9.1 (for the D_2 dopamine receptor).

Among the 720 compounds selected above from the general library, several are likely to display GPCR-binding features. As a consequence for model validation

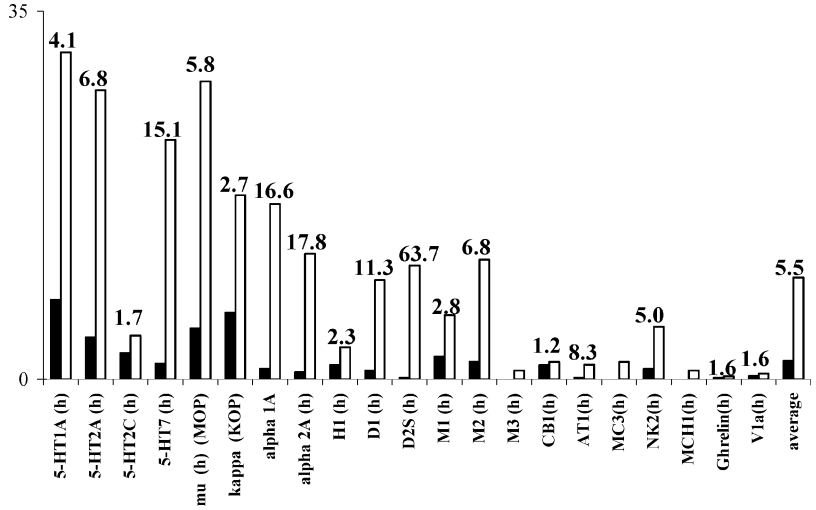

Figure 3. Experimental binding results—at 70% of inhibition at 10 μM—of the 960 compounds (partitioned into "GPCR-predicted" and "non-GPCR-predicted") on 21 GPCRs. The graph compares the hit rates of the set of 360 GPCR-predicted compounds (white bars) with respect to those of the set of 600 non-GPCR-predicted compounds (black bars) on each receptor (enrichment factors added atop of each pair of columns, excepted for receptors for which there were no hits on the non-GPCR-predicted series).

purposes, the 960 compounds (corresponding to the 720 "general" compounds plus the 240 compounds from the GPCR set) were partitioned into "predicted actives" (360 compounds with predicted global $pIC_{50} \geq 4.0$) and "predicted inactives" (600 compounds with global $pIC_{50} < 4.0$). Figure 3 compares the hit rates of the two compound categories, with a clear predominance of hits within the set of "predicted GPCR actives" (13.6%), e.g. 5.7 times more than found among the "predicted inactives" (2.4%). Taken individually, the hit rate enhancement ranged from 1.7- up to 63.7-fold (receptors 5-HT_{2c} and D_2, respectively). In the case of M_3, only the "predicted active" set displayed hits.

To assess the prediction ability of the model on receptors having few hits or totally absent from the initial BioPrint dataset, the initial panel of receptors was completed with seven additional GPCRs belonging to subfamilies A3, A5, A6, A7, A9 and A13: MC_3, AT_1, CB_1, V_{1a}, MCH-1, NK_2, and Ghrelin receptors (the latter three receptors being absent in BioPrint). This led to the definition of an *extended* validation panel, consisting in 21 GPCRs from 10 different subgroups including amine, peptide, and lipid receptors. The results on the 21 GPCRs are presented in Figure 3 with a cutoff set at 70% inhibition at 10 μM. The average hit rate for the set of "predicted actives" reached 9.7%, which corresponds to a 5.5-fold enrichment relative to the "predicted inactives".

Figure 4 shows that the average hit rate enrichment for peptidic GPCRs was consistent with respect to the extended set (5.8-fold versus 5.5-fold, respectively). Among the peptidic GPCRs, the enrichment was particularly important for MC_3 and MCH-1 receptors, for which hits were found only in the set of predicted actives.

These results support the notion that the global GPCR model can be used to enhance hit rates on GPCRs which were not used to build it and raises the potential interest of such a model for the discovery of molecules active on orphan GPCRs.

The comparison of the hit rate enhancement for the set of predicted active at three different percentages of

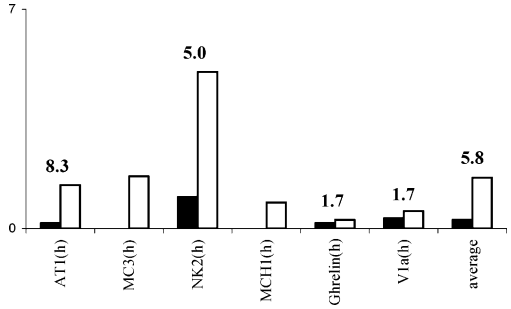

Figure 4. Experimental binding results of the 960 compounds on peptide receptors from the different subgroups of the GPCR family. The graph compares the hit rates of the set of 360 GPCR-predicted compounds (white bars) with respect to those of the set of 600 non-GPCR-predicted compounds (black bars) on each receptor, at 70% of inhibition at 10 μM (enrichment factors added atop of each pair of columns except for MC3 and MCH1, since there were no hits on the non-GPCR-predicted series).

inhibition thresholds (Figure 5a) showed that higher enrichments were obtained with respect to the more potent hits, suggesting that the model favored indeed the most robust hits. Relative enrichment in compounds binding to several receptors is also stronger, as suggested in Figure 5b. For each inhibition threshold value, the enrichments were higher for compounds "hitting" more than three receptors than for compounds "hitting" more than one receptor, reaching in the latter case 18.3-fold at 90% inhibition. The same trends were observed with the panel of the six peptide GPCRs and CB_1 receptor taken separately (Figure 5c,d): (i) higher hit rate enhancement at higher inhibition cutoff and (ii) hit rate enhancement increasing from 1.5- to 9-fold when comparing the compounds hitting at least one (Figure 5c) or three receptors (Figure 5d) at 50% inhibition. This latter observation is most likely a consequence of the methodology used for model building, which focuses on average pIC_{50}s rather than on individual affinity for each receptor.

Using a model based on average pIC_{50} values raises immediately the issue of specificity. A critical aspect was to verify if the molecules selected by the model are not promiscuous compounds binding to GPCRs in an un-

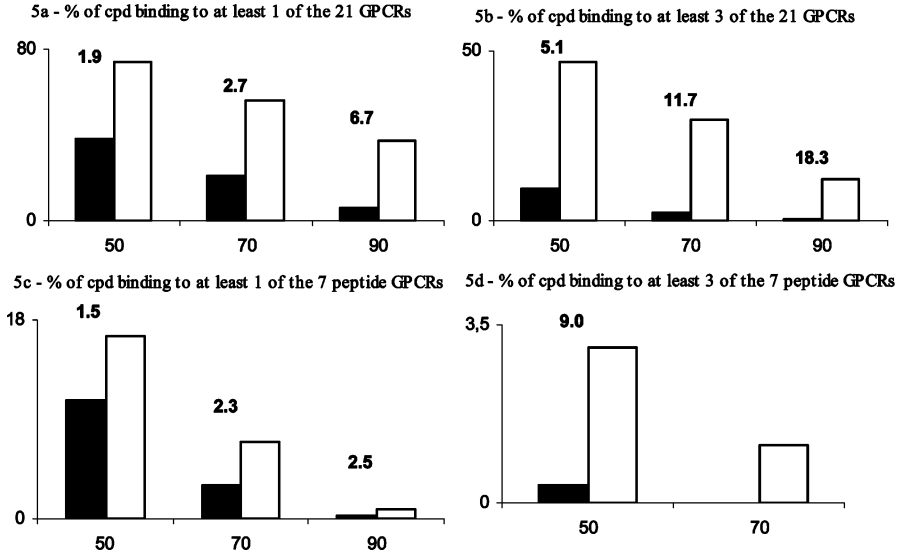

Figure 5. Percentage of molecules binding with at least one receptor (out of 21 in part a and out of seven peptide receptors in part c) or at least three receptors (out of 21 in part b and out of seven peptide receptors in part d) at 10 μM for the sets of predicted actives versus predicted inactives, where the lower inhibition threshold required for a compound to be considered a binder is variable (50, 70, or 90% respectively).

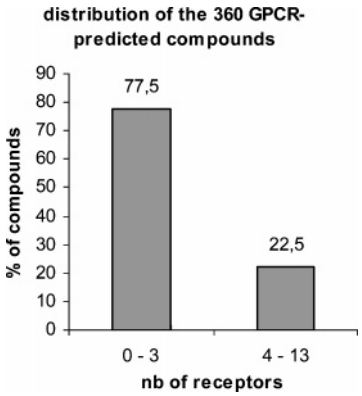

Figure 6. Distribution of the 360 GPCR-predicted compounds according to the number of receptors they hit (with at least 70% of inhibition at 10 μmol), among the 21 receptors of the validation set.

distinguishable fashion but rather compounds with affinity for a limited number of receptors. Therefore, we have analyzed the number of receptors hit by each of the 360 GPCR-predicted compounds synthesized and tested *in vitro* (see Figure 6). Only 22.5% are found active on more than three receptors (out of 21). Less than 9% hit more than seven receptors.

On the other hand, GPCR-focused libraries are intended for HTS and MTS purposes to provide chemists with new hits for drugable or orphan GPCR's. For such an objective, a model able to identify "privileged structures"[21] around which focused libraries are then synthesized is of greater interest than individual QSAR models aiming at the identification of very specific ligands.

As an illustration, we show in the next section that compounds sharing the same "privileged structure" can display very different activity profiles on a panel of GPCR's.

From Privileged Structures to Specific Ligands. Our model selects preferentially compounds with high average affinity for multiple GPCRs, i.e., "privileged" templates binding GPCRs.[21] We have explored whether

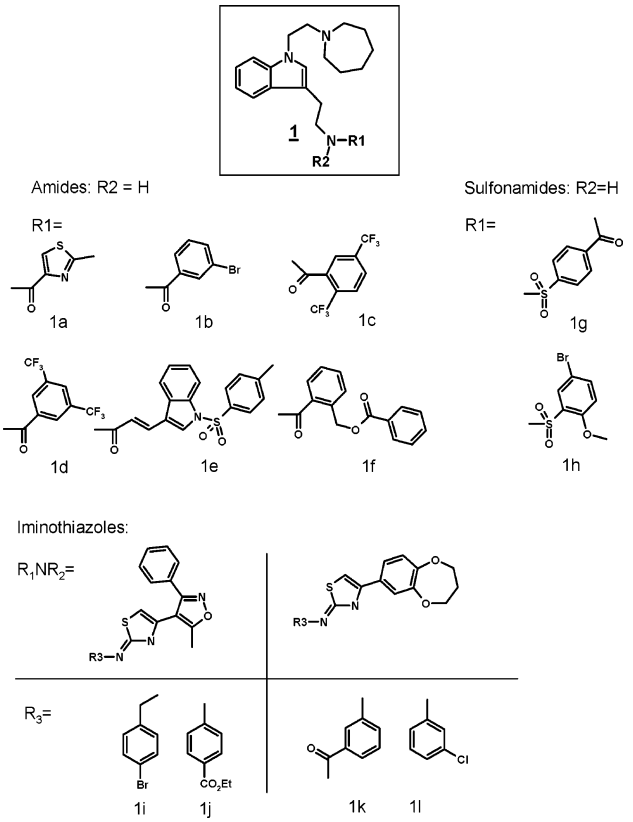

Figure 7. Structures with a common scaffold that are predicted as GPCR-active by the model.

the pharmacological specificity of these templates could be modulated by introducing structural diversity elements on these structures.

An example of a privileged template identified by the model is the 1-(homopiperidin-1-yl) ethylindole scaffold **1** (Figure 7). Among the 960 compounds tested, 12 compounds shared this scaffold and all of them were predicted to be GPCR-active by the model, with predicted average pIC_{50}s between 4.3 and 5.2. Although it is not surprising that scaffold **1** has GPCR binding properties,[22] it is noteworthy that among these 12

Table 3. Binding Profiles (percentages of inhibition at 10 μM) of 12 Compounds Sharing the Same Compound Structure (see Figure 6)

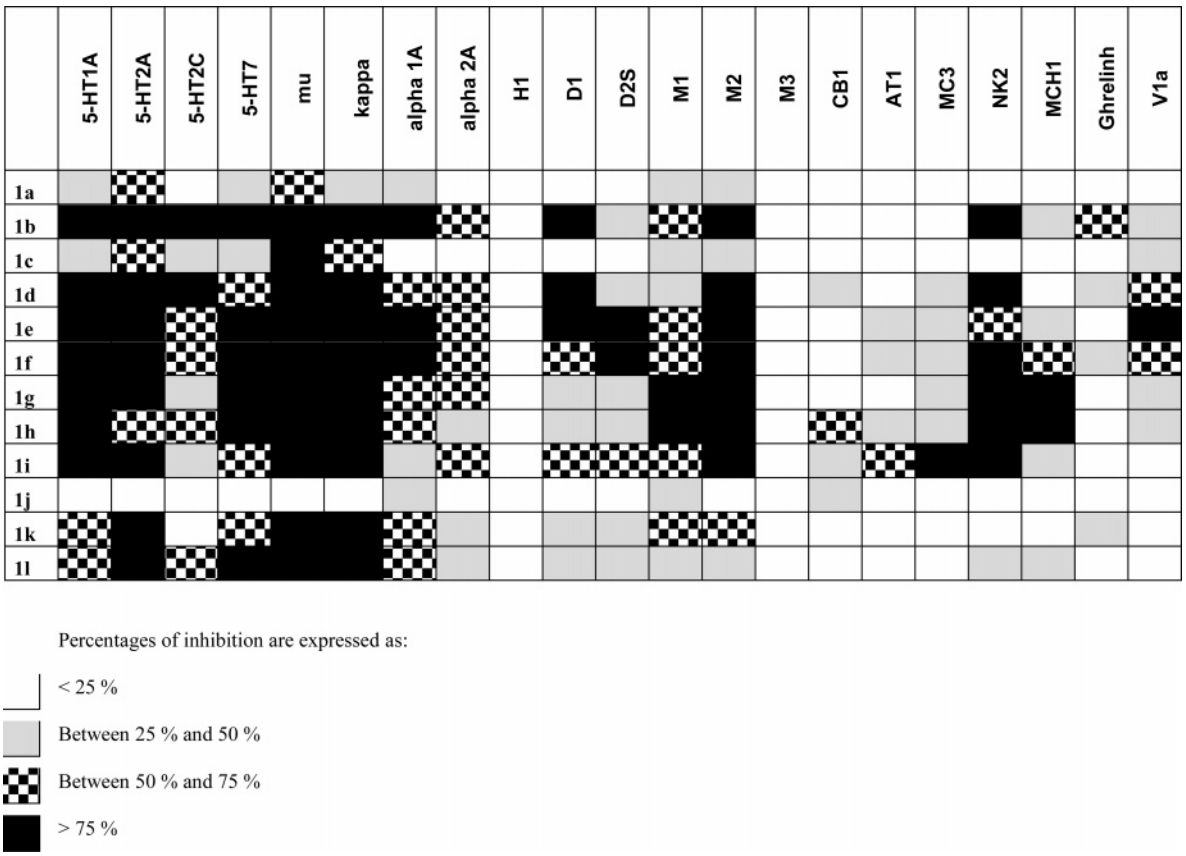

compounds a large variety of binding profiles was obtained depending on the diversity introduced at the nitrogen of the tryptamine moiety (R1, R2). The structures of the compounds are shown in Figure 7, and the corresponding binding profiles (percentages of inhibition at 10 μM) in Table 3.

Among the six amides (**1a**−**f**), the 2-methylthiazole-1-carboxamide (**1a**) and the 2,5-bis(trifluoromethyl)-benzamide (**1c**) display a rather specific profile (Table 3), hitting few GPCRs (μ and 5-HT_{2A} for **1a**, μ and κ for **1c**). On the other hand, amides **1d**−**f** hit many more receptors. Comparison between **1c** and **1d**, which differ only by the position of a trifluoromethyl group, showed that a slight modification around a privileged structure can lead to a significant change in profile. These amide derivatives hit mainly aminergic GPCRs but also three out of the six peptide GPCRs: NK_2, MCH-1, and V1a.

Again, the two sulfonamides **1g** and **1h** hit several aminergic GPCRs, NK_2 and MCH-1, but they are not active on V1a.

Finally, the four related iminothiazole derivatives (**1i**−**l**) displayed very different profiles, since **1j** did not hit any of the 21 GPCRs tested, while its 4-chloro analogue **1i** hit not only aminergic receptors but also two peptide GPCRs (NK_2 and MC-3). On the other hand, **1k** and **1l** hit no peptide GPCRs.

Interestingly, even if **1** is a template that one could assume to be particularly relevant to identify hits on monoaminergic receptors such as 5HT, Table 3 shows that it is also a very useful template to identify new hits on peptide receptors, as for example V1a.

These results suggest that while the model identifies privileged scaffolds binding potentially to a large spectrum of GPCRs, the specific chemical modifications around these templates provide elements of specificity.

Relevance of the Global Model toward Peptide and Chemokine Receptors. Due to the specific properties of peptidic GPCRs, we checked the ability of our model to detect templates acting specifically on peptide and chemokine GPCRs.[23,24] For that purpose, we challenged the model with a set of 69 compounds recently described as ligands for MC-1, MC-3, MC-4, MCH-1, UII, sst1−3, CCR1−5, and CXCR1−2 receptors (diverse chemotypes were selected for each receptor) (Chart 1). Seven out of eight ligands of MC-1, -3, and -4 were predicted as actives, as well as eight out of nine MCH-1 ligands, seven out of eight somatostatin receptor ligands, four out of four urotensin II receptor ligands, and 21 out of 31 CCR1, 2, 3, 5 ligands. Lower prediction rates were obtained with CXCR1/CXCR2 and CCR4 (1/9). Hypothetically, the low prediction rate achieved in the latter cases might be due to the specific structural features of the binding site of CXCR1/CXCR2 and CCR4.[25]

The model is thus able to detect ligands that are described in the literature, but it is mainly intended to reveal original new GPCR ligands. As an illustration, Figure 8 shows some examples of GPCR-predicted compounds that we found active on NK_2 and MCH-1 receptors, respectively (percentage of inhibition higher than 70%), despite their dissimilarity with the commonly described pharmacophores for these targets: no

Chart 1. GPCR Ligands Described in Recent Literature

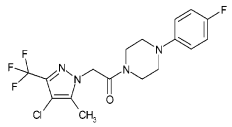

WO 03105853 (Chemo Centryx)
Receptor CCR1
Predicted pIC50 = 3.68

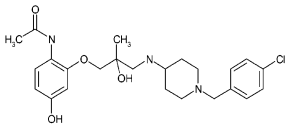

WO 03051839 (Astra Zeneca)
Receptor CCR1
Predicted pIC50 = 4.48

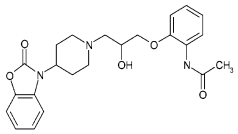

WO 0274763 (Astra Zeneca)
Receptor CCR1
Predicted pIC50 = 4.38

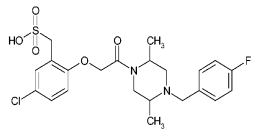

WO 02102787 (Pfizer)
Receptor CCR1
Predicted pIC50 = 3.77

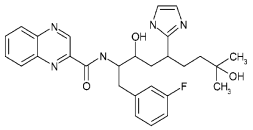

WO 0157023 (Pfizer)
Receptor CCR1
Predicted pIC50 = 3.68

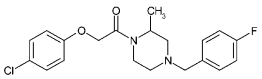

WO 9856771 (Berlex)
Receptor CCR1
Predicted pIC50 = 4.43

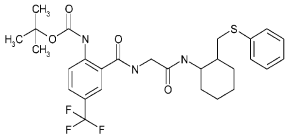

WO 03075853 (Bristol Myers Squibb)
Receptor CCR2
Predicted pIC50 = 3.84

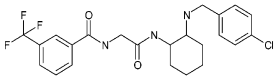

WO 0260859 (Bristol Myers Squibb)
Receptor CCR2
Predicted pIC50 = 4.18

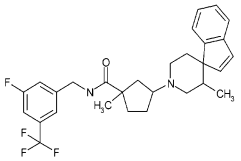

WO 0213824 (Merck)
Receptor CCR2
Predicted pIC50 = 4.37

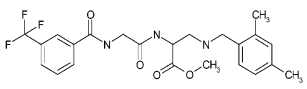

WO 0250019 (Bristol Myers Squibb)
Receptor CCR2
Predicted pIC50 = 4.18

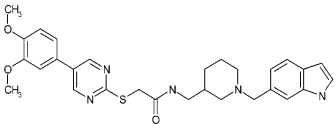

WO 04004731 (Roche)
Receptor CCR3
Predicted pIC50 = 4.47

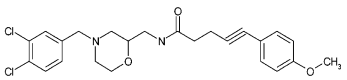

WO 03099798 (Glaxo Smith Kline)
Receptor CCR3
Predicted pIC50 = 4.37

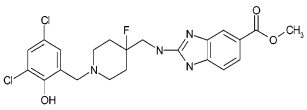

WO 03091245 (Teijin)
Receptor CCR3
Predicted pIC50 = 4.37

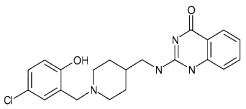

WO 03087089 (Teijin)
Receptor CCR3
Predicted pIC50 = 4.40

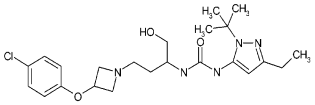

WO 03077907 (Novartis)
Receptor CCR3
Predicted pIC50 = 4.14

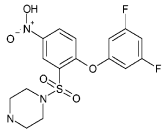

WO 03022277 (Bayer)
Receptor CCR3
Predicted pIC50 = 4.32

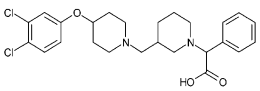

WO 03078421 (Astra Zeneca)
Receptor CCR3
Predicted pIC50 = 4.19

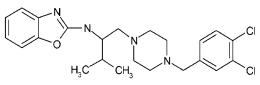

WO 03068759 (Glaxo Smith Kline)
Receptor CCR3
Predicted pIC50 = 4.43

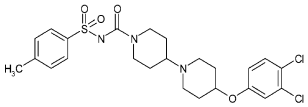

WO 03018556 (Astra Zeneca)
Receptor CCR3
Predicted pIC50 = 3.82

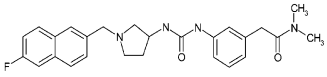

WO 03072545 (Toray/Yamanouchi)
Receptor CCR3
Predicted pIC50 = 4.58

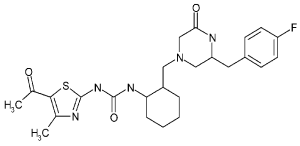

WO 03024401 (Bristol Myers Squibb)
Receptor CCR3
Predicted pIC50 = 3.69

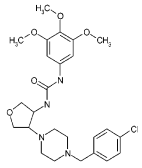

WO 03045917 (Roche)
Receptor CCR3
Predicted pIC50 = 4.17

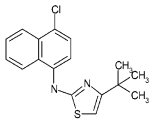

US 2003018022 (Tularik)
Receptor CCR4
Predicted pIC50 = 3.80

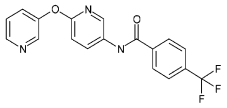

WO 0046203 (Millenium)
Receptor CCR4
Predicted pIC50 = 3.64

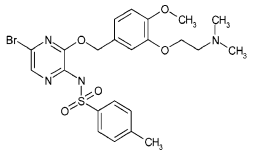

WO 04007472 (ONO)
Receptor CCR4
Predicted pIC50 = 3.66

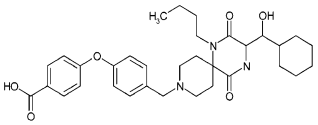

Demarest et al. 11th Conf. Retroviruses
(Glaxo Smith Kline)
Receptor CCR5
Predicted pIC50 = 3.62

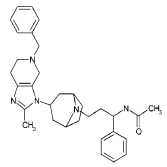

WO 03084954 (Pfizer)
Receptor CCR5
Predicted pIC50 = 4.37

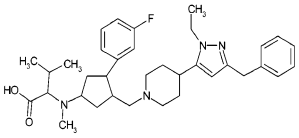

Veazey et al. J. Exp. Med. 2003, 19,
1551
(Merck)
Receptor CCR5
Predicted pIC50 = 4.36

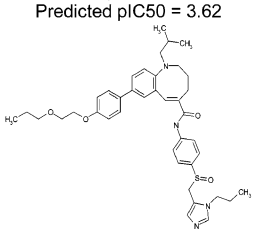

WO 03014110 (Takeda)
Receptor CCR5
Predicted pIC50 = 3.61

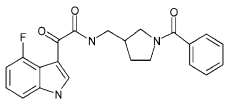

WO 03068281 (Bristol Myers Squibb)
Receptor CCR5
Predicted pIC50 = 4.01

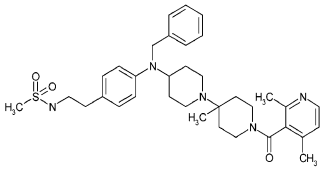

WO 03020716 (Schering Plough)
Receptor CCR5
Predicted pIC50 = 4.52

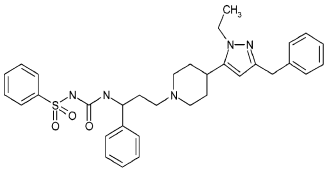

US 6511994 (Merck)
Receptor CCR5
Predicted pIC50 = 3.87

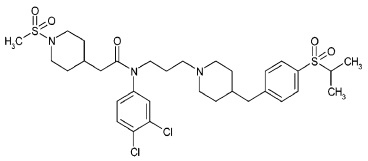

JP 2002138080 (Takeda)
Receptor CCR5
Predicted pIC50 = 4.40

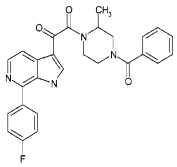

WO 0262423 (Bristol Myers Squibb)
Receptor CCR5
Predicted pIC50 = 3.88

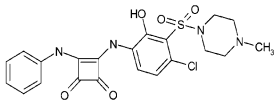

WO 0257230 (Glaxo Smith Kline)
Receptor CXCR1/CXCR2
Predicted pIC50 = 4.10

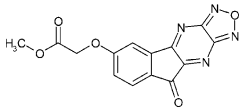

WO 0179209 (Pfizer)
Receptor CXCR1/CXCR2
Predicted pIC50 = 3.54

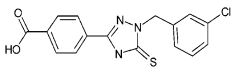

WO 0177087 (Astra Zeneca)
Receptor CXCR1/CXCR2
Predicted pIC50 = 3.62

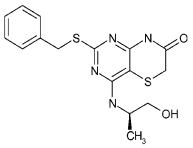

WO 0162758 (Astra Zeneca)
Receptor CXCR1/CXCR2
Predicted pIC50 = 3.87

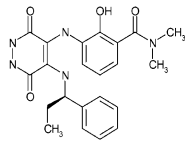

WO 03057676 (Schering Plough)
Receptor CXCR1/CXCR2
Predicted pIC50 = 3.62

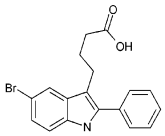

WO 0138305 (Fournier)
Receptor CXCR1/CXCR2
Predicted pIC50 = 3.78

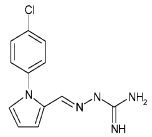

WO 03013509 (Melacure)
Receptor MC-1
Predicted pIC50 = 4.06

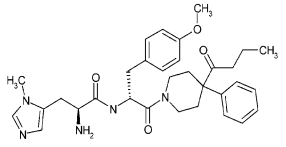

WO 02069905 (Bristol Myers Squibb)
Receptor MC-1
Predicted pIC50 = 3.95

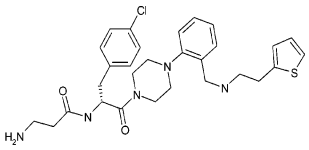

WO 03094918 (Neurocrine)
Receptor MC-3
Predicted pIC50 = 4.26

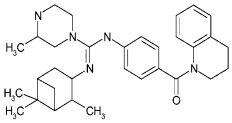

WO 03066597 (Chiron)
Receptor MC-4
Predicted pIC50 = 4.09

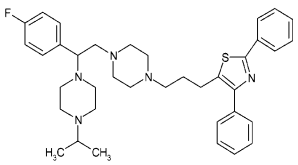

WO 03053927 (Taisho)
Receptor MC-4
Predicted pIC50 = 4.70

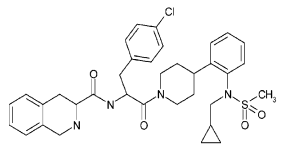

WO 03009847 (Amgen)
Receptor MC-4
Predicted pIC50 = 4.16

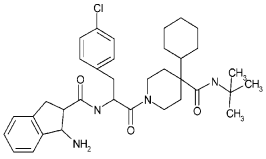

WO 0215909 (Merck)
Receptor MC-4
Predicted pIC50 = 4.06

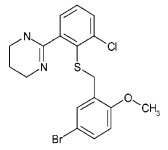

WO 0110842 (Millenium)
Receptor MC-4
Predicted pIC50 = 4.00

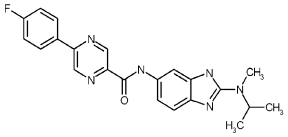

WO 04011440 (Banyu)
Receptor MCH-1
Predicted pIC50 = 3.94

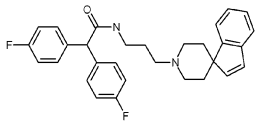

WO 04004714 (Synaptic)
Receptor MCH-1
Predicted pIC50 = 4.69

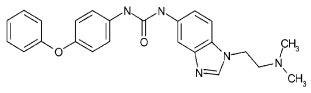

WO 03015769 (Aventis)
Receptor MCH-1
Predicted pIC50 = 4.02

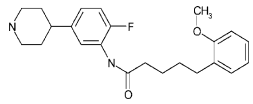

WO 04005257 (Synaptic)
Receptor MCH-1
Predicted pIC50 = 4.25

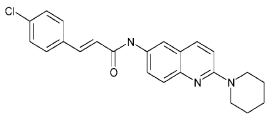

WO 03045313 (Merck)
Receptor MCH-1
Predicted pIC50 = 4.64

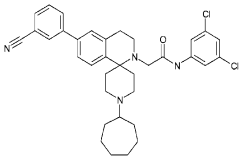

WO 04002987 (Schering Plough)
Receptor MCH-1
Predicted pIC50 = 4.88

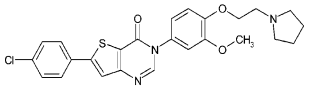

WO 03033476 (Glaxo Smith Kline)
Receptor MCH-1
Predicted pIC50 = 4.35

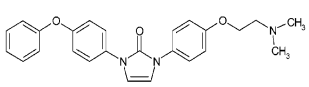

WO 04011438 (Aventis)
Receptor MCH-1
Predicted pIC50 = 4.40

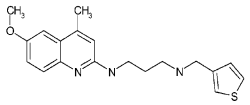

WO 04004726 (Astra Zeneca)
Receptor MCH-1
Predicted pIC50 = 4.34

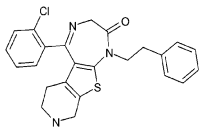

WO 0061587 (SCRAS)
Receptor Somatostatin
Predicted pIC50 = 4.63

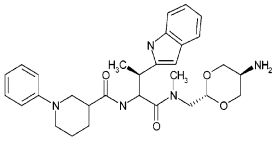

US 6387932 (Merck)
Receptor Somatostatin
Predicted pIC50 = 4.43

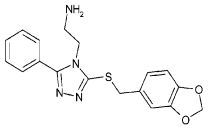

WO 03045926 (SCRAS)
Receptor Somatostatin
Predicted pIC50 = 4.15

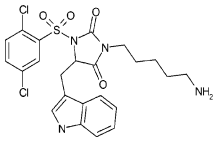

WO 018578 (Novartis)
Receptor Somatostatin
Predicted pIC50 = 4.40

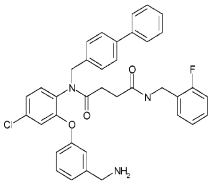

WO 0023420 (Takeda)
Receptor Somatostatin
Predicted pIC50 = 4.38

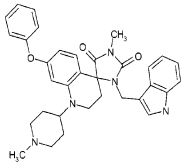

WO 03090677 (Chembridge)
Receptor Somatostatin
Predicted pIC50 = 4.64

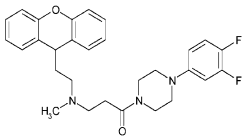

WO 03040125 (Novartis)
Receptor Somatostatin
Predicted pIC50 = 4.36

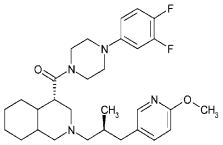

WO 0170731 (Novartis)
Receptor Somatostatin
Predicted pIC50 = 3.96

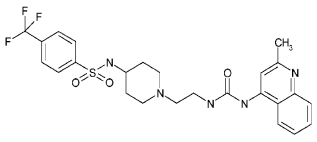

WO 03048154 (Actelion)
Receptor Urotensin II
Predicted pIC50 = 4.20

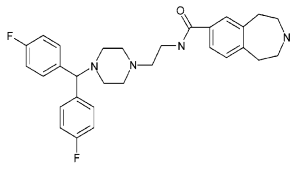

WO 0202530 (Takeda)
Receptor Urotensin II
Predicted pIC50 = 4.73

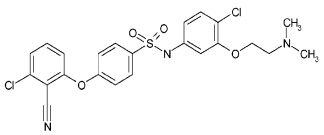

WO 0289785 (Glaxo Smith Kline)
Receptor Urotensin II
Predicted pIC50 = 4.08

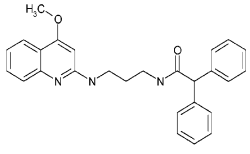

WO 0258702 (Glaxo Smith Kline)
Receptor Urotensin II
Predicted pIC50 = 4.24

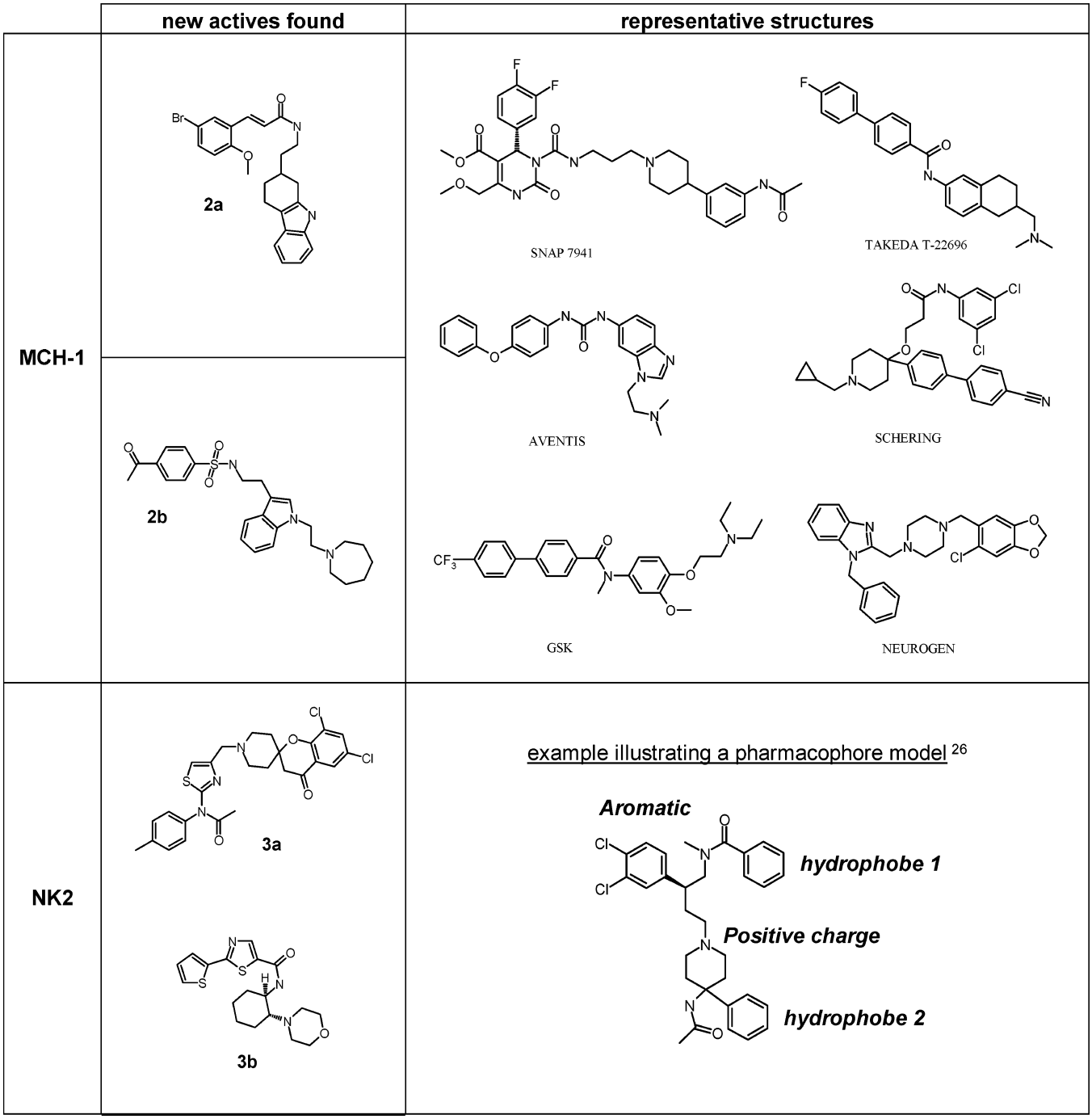

Figure 8. Compounds of the GPCR library compared to representative structures for two peptide receptors.

positive charge in the molecule **2a**, while it appears in all known MCH-1 ligands and no typical NK related "central nitrogen/two final aromatic ring systems" pattern in the aminothiazole molecule **3b**.

Conclusion

A predictive model capturing critical structural features for GPCR binding was built on the basis of a large experimental standardized profiling dataset. The prediction ability of the model was evaluated by synthesizing and testing a collection of GPCR-predicted compounds on a large series of GPCRs from different families, thus experimentally validating our approach. To our knowledge, this is the most extensive experimental validation of a GPCR focused library.

Significant hit rate enhancements were obtained not only for the receptors present in the database but for a wide array of other GPCRs, including peptide receptors.

Such an approach could have a general value and be utilized for other target families (enzymes or receptors). It should allow identification of new privileged scaffolds for each of these families and understanding how specific structural modulations provide pharmacological selectivity and specificity.

Experimental Section

In Vitro Assays Experimental Protocol. Evaluation of the affinities of compounds for each receptor was determined in radioligand binding assays, performed

following standard operating procedures (details provided in the Supporting Information).

Protocols for binding assays included a minimum of eight control wells (nonspecific and total) and a standard reference compound that was tested in each experiment at several concentrations to obtain a competition curve from which its IC_{50} was calculated. Total binding was determined in the presence of the vehicle of test compounds. Nonspecific binding was determined in the presence of an excess of an appropriate compound.

Membrane homogenates were incubated with a determined concentration of the appropriate radioligand in the absence or presence of the test compound. Following the incubation, the samples were filtered rapidly under vacuum through glass fiber filters, dried, and then counted for radioactivity in a scintillation counter using a scintillation cocktail. The results were expressed as a percent inhibition of the control radioligand specific binding.

Supporting Information Available: Details of the experimental procedures of the various in vitro assays. This material is available free of charge via the Internet at http://pubs.acs.org.

References

(1) Drews, J. Drug discovery: A historical perspective. *Science* **2000**, *287*, 1960−1964.

(2) Klabunde T.; Hessler G. Drug design strategies for targeting G-protein-coupled receptors. *ChemBioChem* **2002**, *3* (10), 928−944.

(3) Probst W. C.; Snyder L. A.; Schuster D. I.; Brosius J.; Sealfon S. C. Sequence alignment of the G-protein coupled receptor superfamily. *DNA Cell. Biol.* **1992**, *11* (1), 1−20.

(4) Joost, P.; Methner, A. Phylogenetic analysis of 277 human G-protein-coupled receptors as a tool for the prediction of orphan receptor ligands. *Genome Biol.* **2002**, *3* (11), 0063.1−0063.16. (http://genomebiology.com/2002/3/11/research/0063).

(5) Palczewski, K.; Kumasaka, T.; Hori, T.; Behnke, C. A.; Motoshima, H.; Fox, B. A.; Le Trong, I.; Teller, D. C.; Okada, T.; Stenkamp, R. E.; Yamamoto, M.; Miyano**,** M. Crystal structure of rhodopsin: A G protein-coupled receptor. *Science* **2000**, *289* (5480), 739−745.

(6) Becker, O. M.; Shacham, S.; Marantz, Y.; Noiman, S. Modeling the 3D structure of GPCRs: Advances and application to drug discovery. *Curr. Opin. Drug Discov. Devel.* **2003**, *6* (3), 353−361.

(7) Bissantz, C.; Bernard, Ph.; Hibert, M.; Rognan, D. Protein-based virtual screening of chemical databases. II. Are homology models of G-protein coupled receptors suitable targets? *Proteins* **2003**, *50* (1), 5−25.

(8) Archer, E.; Maigret, B.; Escrieut, Ch.; Pradayrol, L.; Fourmy, D. Rhodopsin crystal: new template yielding realistic models of G-protein-coupled receptors? *Trends Pharmacol. Sci.* **2003**, *24* (1), 36−40.

(9) Krejsa, C. M.; Horvath, D.; Rogalski, S. L.; Penzotti, J. E.; Mao, B.; Barbosa, F.; Migeon, J. C. Predicting ADME properties and side effects: the BioPrint approach. *Curr. Opin. Drug Discovery Dev.* **2003**, *6* (4), 470−480.

(10) Gozalbes, R.; Barbosa, F.; Froloff, N.; Horvath, D. The BioPrint approach for the evaluation of ADME-T properties: Application to the prediction of cytochrome P450 2D6 inhibition. Proceedings of the LogP symposium, 2004, submitted.

(11) Horvath, D. High throughput conformational sampling and fuzzy similarity metrics: a novel approach to similarity searching and focused combinatorial library design and its role in the drug discovery laboratory. In *Combinatorial Library Design and Evaluation: Principles, Software Tools and Applications in Drug Discovery;* Ghose, A., Viswanadhan, V., Eds.; Marcel Dekker: New York, 2001; pp 429−472.

(12) Horvath, D.; Jeandenans, C. Neighborhood behavior of in silico structural spaces with respect to in vitro activity spaces—A novel understanding of the molecular similarity principle in the context of multiple receptor binding profiles. *J. Chem. Inf. Comput. Sci.* **2003**, *43* (2), 680−690.

(13) Horvath, D.; Jeandenans, C. Neighborhood behavior of in silico structural spaces with respect to in vitro activity spaces—A benchmark for neighborhood behavior assessment of different in silico similarity metrics. *J. Chem. Inf. Comput. Sci.* **2003**, *43* (2), 691−698.

(14) Todeschini, R.; Consonni, V. In *Handbook of Molecular Descriptors*; Mannhold, R., Kubinyi, H., Timmerman, H., Eds.; Wiley-VCH: 2000, 464−466.

(15) Oprea, TI. Chemical space navigation in lead discovery. *Curr. Opin. Chem. Biol.* **2002**, *6* (3), 384−389.

(16) Patterson, D. E.; Cramer, R. D.; Ferguson, A. M.; Clark, R. D.; Weinberger, L. E. Neighborhood behavior: A useful concept for validation of "molecular diversity" descriptors. *J. Med. Chem.* **1996**, *39*, 9 (16), 3049−3059.

(17) Holenz, J.; Merce, R.; Diaz, J. L.; Guitart, X.; Codony, X.; Dordal, A.; Romero, G.; Torrens, A.; Mas, J.; Andaluz, B.; Hernandez, S.; Monroy, X.; Sanchez, E.; Hernandez, E.; Perez, R.; Cubi, R.; Sanfeliu, O.; Buschmann, H. Medicinal chemistry driven approaches toward novel and selective serotonin 5-HT6 receptor ligands. *J. Med. Chem*. **2005**, *48* (6), 1781−1795.

(18) Moro, S.; Braiuca, P.; Deflorian, F.; Ferrari, C.; Pastorin, G.; Cacciari, B.; Baraldi, P. G.; Varani K.; Borea, P. A.; Spalluto, G. Combined target-based and ligand-based drug design approach as a tool to define a novel 3D-pharmacophore model of human A3 adenosine receptor antagonists: Pyrazolo[4,3-*e*]1,2,4-triazolo[1,5-*c*]pyrimidine derivatives as a key study. *J. Med. Chem*. **2005**, *48* (1), 152−162.

(19) Evers, A.; Klebe, G. Successful virtual screening for a submicromolar antagonist of the neurokinin-1 receptor based on a ligand-supported homology model. *J. Med. Chem*. **2004**, *47* (22), 5381−5392.

(20) Sun, H.; Greeley, D. N.; Chu, X. J.; Cheung, A.; Danho, W.; Swistok, J.; Wang, Y.; Zhao, C.; Chen, L.; Fry, D. C. A predictive pharmacophore model of human melanocortin-4 receptor as derived from the solution structures of cyclic peptides. *Bioorg. Med. Chem.* **2004**, *12* (10), 2671−2677.

(21) Bondensgaard, K.; Ankersen, M.; Thøgersen, H.; Hansen, B. S., Wulff, B. S., Bywater, R. P. Recognition of privileged structures by G-protein coupled receptors. *J. Med. Chem.* **2004**, *47* (4), 888−899.

(22) Hipskind, P. A.; Lobb, K. L.; Nixon, J. A.; Britton, T. C.; Bruns, R. F.; Catlow, J.; Dieckman-McGinty, D. K.; Gackenheimer, S. L.; Gitter, B. D.; Iyengar, S.; Schober, D. A.; Simmons, R. M.; Swanson, S.; Zarrinmayeh, H.; Zimmerman, D. M.; Gehlert, D. R. Potent and selective 1,2,3-trisubstituted indole NPY Y-1 antagonists. *J. Med. Chem.* **1997**, *40*, (23), 3712−3714.

(23) Gurrath M. Peptide-binding G protein-coupled receptors: New oportunities for drug design. *Curr. Med. Chem.* **2001**, *8* (13), 1605−1648.

(24) Baggiolini, M. Chemokines in pathology and medicine. *J. Intern. Med.* **2001**, *250* (2), 91−104.

(25) Lindow, M.; Lüttichau, H. R.; Schwartz, T. W. Viral leads for chemokine-modulatory drugs. *Trends Pharmacol. Sci.* **2003**, *24* (3), 126−130.

(26) Poulsen, A.; Liljefors, T.; Gundertofte, K.; Bjørnholm, B. A pharmacophore model for NK2 antagonist comprising compounds from several structurally diverse classes. *J. Comput.-Aided Mol. Des.* **2002**, *16*, 273−286.

JM0500673